Characterization of Laminar Damage in an Aluminium Panel by Diffraction Tomography Based Imaging Method Using Lamb Waves

Eugene Chan, Chun H. Wang, Francis L.R. Rose

7th European Workshop on Structural Health Monitoring
July 8-11, 2014. La Cité, Nantes, France

CHARACTERISATION OF LAMINAR DAMAGE IN AN ALUMINIUM PANEL BY DIFFRACTION TOMOGRAPHY BASED IMAGING METHOD USING LAMB WAVES

Eugene Chan[1], Chun H. Wang[1*], L. R. Francis Rose[1]

[1] *Sir Lawrence Wackett Aerospace Research Centre, School of Aerospace, Mechanical and Manufacturing Engineering, RMIT University, GPO Box 2476, Melbourne, Victoria 3001, Australia*

[*]chun.wang@rmit.edu.au

ABSTRACT

Most of the research on Structural Health Monitoring employs guided waves only to detect and locate damage in a plate-like structure. The purpose of this paper is to present a Diffraction Tomography based imaging method, using experimentally-determined scattered fields and numerically computed Green's functions, to characterise laminar damage in an aluminium panel. The approach is based on a recently derived extension of diffraction tomography which utilises the multi-static scattering matrix constructed from the measurements of the scattered field for every source and receiver pair, as well as the Green's function of the structure. The imaging results have provided an accurate characterisation of damage geometry and size derived from experimental data. These results are shown to compare favourably with those obtained from computational data.

KEYWORDS : *Guided waves, Inverse problems, Prediction and Estimation by Calculation, Image processing.*

INTRODUCTION

Quantitative characterisation of structural damage is of great importance to the continual assurance of structural integrity of aircraft. With information about location, geometry, size and severity of the damage, the residual strength and fatigue life of the structure can be predicted through established predictive models.

With recent significant progress towards quantitative damage imaging through application of advanced diffraction tomography [1, 2] and time-reversal imaging [3, 4] methods employing Green's function of the structure, which is its response to a point source, it is now possible to obtain quantitative characterisation of the damage in terms of the damage's location, geometry, size and severity.

Using an eigenfunction approach, Rose and Wang [1] were able to characterise damage that can be modelled as a flexural inhomogeneity. More recently, Chan et al. [5] developed a diffraction tomography based generic framework for image reconstruction, and demonstrated the approach using computational model data for a thickness reduction in an isotropic plate. The approach which utilises the Green's function and the multi-static scattering matrix, populated from the measurements of the scattered wave field for every actuator and receiver pair, has been shown to produce an excellent quality image of the damage and hence accurate quantitative characterisation.

The objective of this paper is to extend the work in [1, 5] to the case of experimentally measured data. The resulting image quality is compared with that obtained from computational data. Directions for future work are also indicated.

1 IMAGING SET UP

In the current work, the case of a flat aluminium plate, thickness 1.6 mm and width 600 mm, is considered. The set up consists of a circular network of 16 radially-equispaced surface mounted piezoelectric transducers (PZT), playing the dual role of actuator and receiver. As shown in Figure 1a, the sensor array is located on a radius R = 75 mm with origin at the centre of the aluminium plate and the individual PZTs are numbered from 1 to 16.

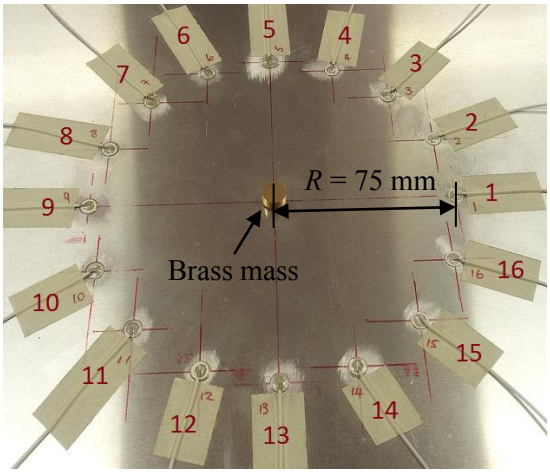

Figure 1a: Aluminium plate with 16 PTZs sensor network and brass mass as laminar damage.

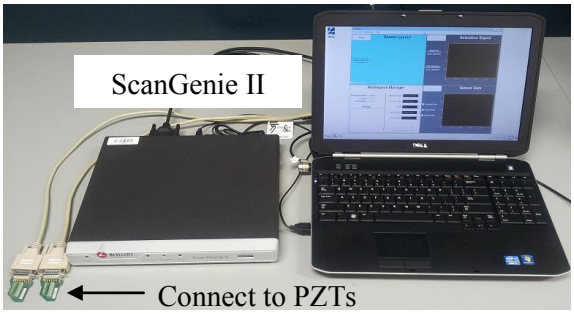

Figure 1b: Data acquisition hardware; 16 pin connector, ScanGenie II system and laptop.

APC International 850 disc type PZTs, diameter 6.35 mm and height 0.254 mm, were employed in the set up. The sensor network was electrically connected to an Acellent Technologies ScanGenie II data acquisition system as illustrated in Figure 1b.

To simulate the effects of thickness and mass reductions due to a laminar damage, a cylindrical brass mass, diameter 10 mm and height 5 mm, is temporarily bonded onto the surface of the plate at the origin with high temperature vacuum bagging sealant as shown in Figure 1a. It is worth noting that the effective diameter of this simulated geometry and property change is less than 10 mm, as the transfer length for wave propagation between the interfaces of the different material types, (aluminium, sealant and brass), and the bond strength is an unknown [6].

2 DATA GATHERING PROCEDURE

In acquiring the voltage signals required for reconstruction of the laminar damage, the data acquisition hardware was used to sequentially interrogate the aluminium plate for every permutation of actuator and receiver pairs. The plate was interrogated twice with a 50V 200 kHz 5-cycle tone burst; once in absence of the brass mass for baseline voltage signals $V_{ij}^{B}(t)$, and a second time with the brass mass attached for total voltage signals $V_{ij}^{T}(t)$. The subscripts i and j refer to the index and hence position of a receiver and actuator respectively.

An example of the baseline signal for i = 9 and j = 1 is shown in Figure 2a. The pulse spanning between 0 and 30 μs is the cross-talk between actuator and receiver channels, while the signal packet between 30 and approximately 60 μs belongs to the fundamental symmetric S_0 mode. In this work, only the A_0 mode arriving at 75.5 μs, (determined with Hilbert Transform), is of interest.

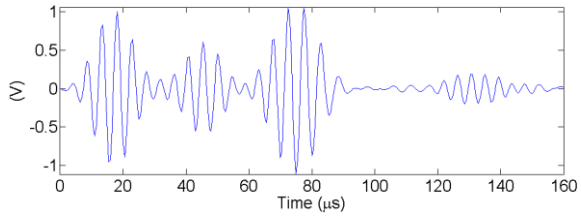

Figure 2a: Baseline signal for $j = 1$ and $i = 9$.

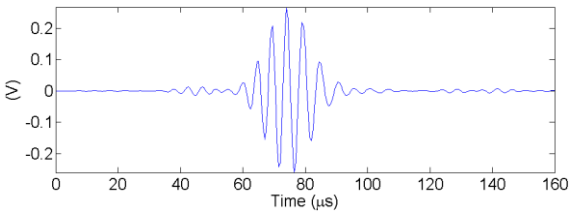

Figure 2b: Scattered signal for $j = 1$ and $i = 9$.

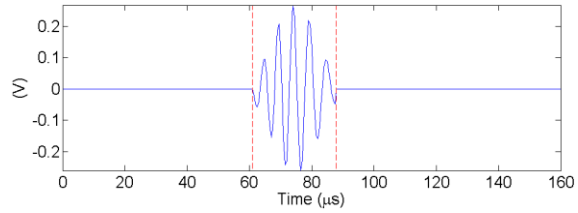

Figure 2c: Windowed scattered signal for $j = 1$ and $i = 9$.

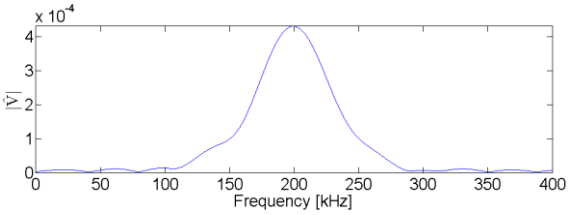

Figure 2d: Frequency-domain windowed scattered signal for $j = 1$ and $i = 9$.

3 DATA PROCESSING PROCEDURE

The key to reconstructing the laminar damage is the scattered wave field voltage signals calculated from baseline subtraction method as,

$$V_{ij}^{S}(t) = V_{ij}^{T}(t) - V_{ij}^{B}(t). \tag{1}$$

Shown in Figure 2b is an example of the scattered signal for $i = 9$ and $j = 1$. To determine the exact arrival time and extract the A_0 mode, Hilbert Transform and a rectangular window of width 25 μs, centred over the arrival time of the pulse, was employed to window and hence remove spurious signals from the scattered voltage-time trace. The windowed scattered signal for the same index ij is shown is Figure 2c where the vertical dash-lines represent the boundaries of the window.

In implementing the imaging formula, the complex valued frequency-domain signal $\hat{V}_{ij}^{S}$ at input frequency of 200 kHz is used, instead of the time-domain version. Figure 2d shows the Discrete Fourier Transform version of Figure 2c.

4 IMAGING FORMULA

The diffraction tomography based imaging formula employed in this work to produce the imaging result is given as [5, 7],

$$s_{MDT}(\mathrm{x}) = \mathrm{Re}\left[-\frac{B}{8\pi^2} \sum_{j=1}^{N_s} \sum_{i=1}^{N_r} \frac{\hat{V}_{ij}^{S} \left| \sin(\phi_i - \phi_j) \right|}{D\gamma_1 \left(k_1^2 - k_2^2\right) G(\mathrm{x}, \mathrm{X}_j) G(\mathrm{X}_i, \mathrm{x}) q(\phi_i - \phi_j + \pi)} \Delta\phi_i \Delta\phi_j \right], \tag{2}$$

where N_s and N_r denotes the number of sources and receivers respectively, $\hat{V}_{ij}^{S}$ is computed with the procedure outlined in Section 3, and G is the fundamental anti-symmetric wave (A_0) Green's function between an actuator at X_j or a receiver at X_i and imaging point x, the variable φ denotes the polar angle relative to the imaging point x, and other symbols are defined in [5, 7].

Unlike the multi-static scattering matrix derived in the works by Rose et al. [7] and Chan et al. [5], the scattered voltage signal $\hat{V}_{ij}^{S}$ includes the contributions of unknown electro-mechanical transfer functions that are not pursued in this paper [2, 3]. Consequently, the reconstruction predicts

damage size, but the damage severity i.e. height of the brass mass, requires the determination of a scaling constant denoted by B in Equation 2, e.g., through calibration against a known damage.

4.1 Numerical Green's Function

The Green's function in Equation 2 is defined as [5],

$$G(\boldsymbol{x}, \boldsymbol{X}_j) = \frac{\hat{w}^I(\boldsymbol{x}, \omega; \boldsymbol{X}_j)}{\hat{F}(\omega)} \quad , \quad G(\boldsymbol{X}_i, \boldsymbol{x}) = G(\boldsymbol{x}, \boldsymbol{X}_i) = \frac{\hat{w}^I(\boldsymbol{x}, \omega; \boldsymbol{X}_i)}{\hat{F}(\omega)} \tag{3}$$

where $\hat{F}(\omega)$ is the input force and $\hat{w}^I(\boldsymbol{x}, \omega; \boldsymbol{X})$ is the incident transverse plate deflection at imaging point $\boldsymbol{x}$ due to a wave propagated from sensor position $\boldsymbol{X}$. Both input force and plate deflection are complex valued and captured at the input frequency.

The Green's function within an imaging region of interest is computed numerically with displacement data from explicit solver Finite Element (FE) analyses. Figure 3a illustrates the schematic of the FE set up.

In this work, 64 radially-equispaced nodes, located on sensor array radius R, were designated as point actuators. These 64 nodes as shown in Figure 3a, include the actual 16 PZT locations interspersed with a further 48 virtual actuator positions. This number of actuators is chosen so as to satisfy the Nyquist criterion $N = 2kR_0$ [8, 9] for an imaging domain of size with inscribed radius $R_0 = 64/2k = 38$ mm.

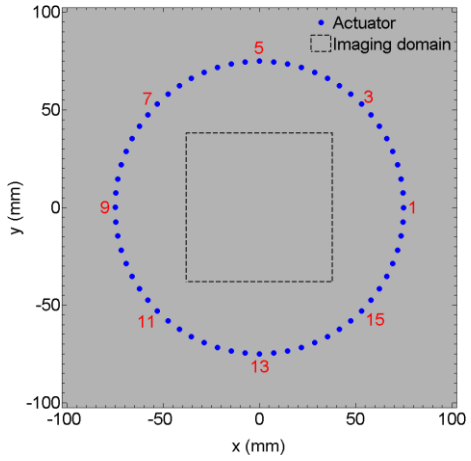

Figure 3a: Schematic of Finite Element set up showing PZT locations numbered 1 to 16.

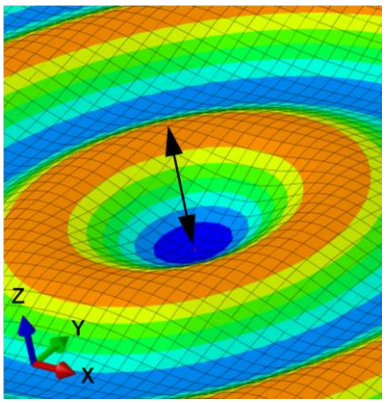

Figure 3b: Illustration of input force on a single node.

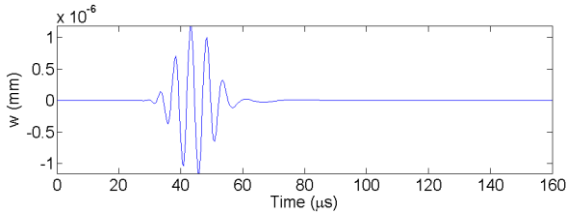

Figure 3c: Displacement-time history for $\boldsymbol{x} = (0,0)$ mm due to wave from actuator $\boldsymbol{X}_{j=1}$.

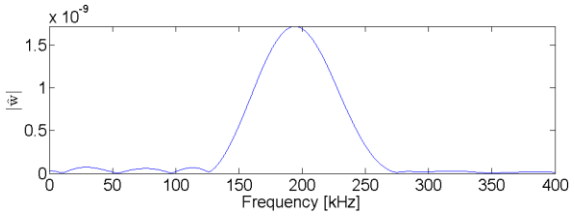

Figure 3d: Frequency-domain signal for $\boldsymbol{x} = (0,0)$ mm due to wave from actuator $\boldsymbol{X}_{j=1}$.

Further, a uniform square grid mesh comprising of shell elements with size 0.5×0.5 mm was employed to simulate mode A_0 wave propagation throughout the aluminium plate having material properties: thickness 1.6 mm, Young's Modulus E = 69 GPa, Poisson ratio ν = 0.33 and density

ρ = 2760 kg/m^3. The plate width in the FE analyses was 400 mm, which was sufficiently large to exclude any signals due to plate edge reflections for a simulation time of 160 μs.

The nominal 5-cycles tone burst that is applied experimentally consists in fact of 5.5 cycles. Accordingly, a 5.5-cycle input tone burst $-\sin(\omega t)$ with vertical force of 1.0 N at 200 kHz was applied on actuator positions in the FE model to initiate mode A_0 wave as shown in Figure 3b.

With an imaging domain size of width 38 mm, the displacement-time history for a total of 153×153 nodes within the grid mesh was extracted at a period of 500 ns. Figure 3c shows an example of the displacement-time history for a wave propagated from actuator $X_{j=1}$ and captured at imaging point x = (0,0) mm. The corresponding frequency-domain signal of Figure 3c is shown Figure 3d.

5 IMAGING RESULTS

Prior to evaluation of the image using Equation 2, the scattered voltage signal $\hat{V}_{ij}^{S}$ is up-sampled from 16×16 to 64×64 matrix through a two-dimensional Piecewise Cubic Hermite Interpolating Polynomial scheme to achieve a $\hat{V}_{ij}^{S}$ matrix size that is similar to the total number of Green's function datasets.

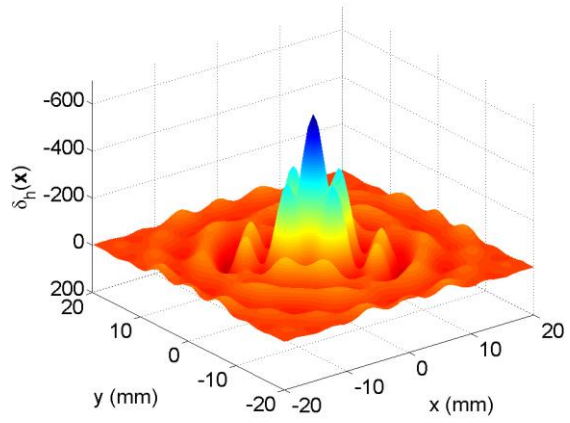

Figure 4a: Three-dimensional variation of the reconstructed laminar damage.

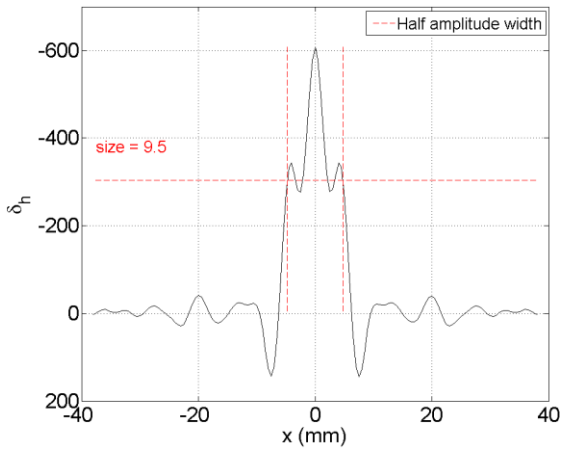

Figure 4b: Profile variation of the reconstructed laminar damage.

Figure 4a shows the three-dimensional variation of the reconstructed laminar damage. It can be seen that a strong peak is formed at the origin, with low-levels of artefacts throughout the imaging domain. This is shown in profile in Figure 4b, which also shows that the predicted size of the laminar damage, measured at the width for half amplitude, is 9.5 mm in diameter. This compares favourably with the actual diameter of 10 mm. As mentioned earlier in Section 1, the effective size of the simulated laminar damage can be expected to be somewhat less than the actual size due to an unknown load transfer length for load transfer through the adhesive layer.

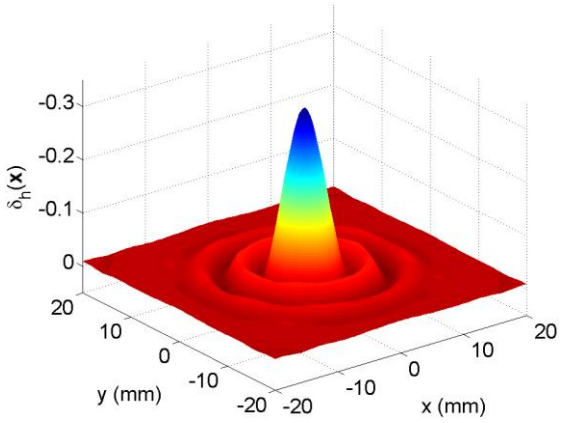

Figure 5a: Three-dimensional variation for an idealised part-through hole using computational data [5].

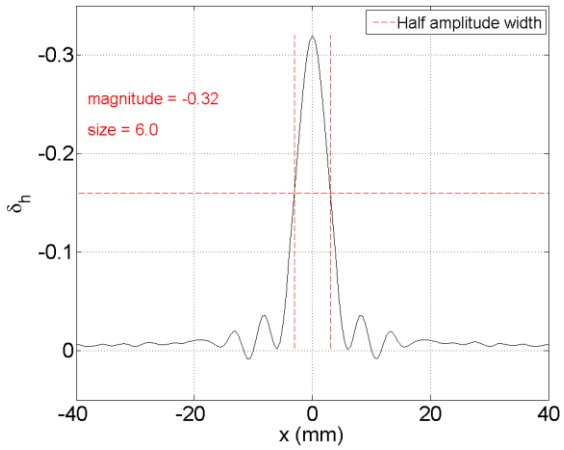

Figure 5b: Profile variation for an idealised part-through hole using computational data [5].

The corresponding reconstruction using computational data for a mid-plane symmetric thickness reduction over a circular region [5] is presented in Figures 5a and 5b. In this case, the predicted geometry is perfectly round and an accuracy of 80% was obtained for size and severity predictions. Despite poorer reconstruction quality when compared with Figure 5, the imaging result obtained from experimental data in this paper is a significant improvement relative to previous work [10-12]. The results shown in Figure 4 are very encouraging, and support the possibility of quantitative characterisation of laminar damage in an actual complex plate-like aerospace structure.

CONCLUSION

In this work, we have demonstrated, the actual implementation of a diffraction tomography based imaging procedure applied to experimental data for laminar damage on an aluminium plate.

The imaging procedure described in the paper, utilised the scattered wave field voltage signals measured experimentally by a network of 16 thin disc PZTs, and numerically computed Green's function datasets. Although the imaging quality is not as good as that obtained with computational data, it is very encouraging and hence shows great potential towards realistic quantitative characterisation of laminar damage.

Further research work is now directed towards quantifying the PZT transfer functions for correct prediction of the damage severity, and improving the prediction performance for size and geometry reconstruction, as well as addressing structural complexities such as the presence of integral stiffeners.

ACKNOWLEDGEMENT

This study was supported in part by an Australian Research Council (ARC) Discovery Grant (DP 120103430). The Ultrasonics Group of The University of Queensland is deeply appreciated for meaningful discussions and provision of the brass mass.

REFERENCES

[1] Rose, L.R.F. and C.H. Wang, *Mindlin plate theory for damage detection: Imaging of flexural inhomogeneities.* The Journal of the Acoustical Society of America, 2010. **127**(2): p. 754-763.

[2] Rose, L.R.F. and C.H. Wang, *Mindlin plate theory for damage detection: Source solutions.* The Journal of the Acoustical Society of America, 2004. **116**(1): p. 154-171.

[3] Wang, C.H., J.T. Rose, and F.K. Chang, *A synthetic time-reversal imaging method for structural health monitoring.* Smart Materials and Structures, 2004. **13**(2): p. 415.

[4] Chan, E., C.H. Wang, and L.R.F. Rose, *Characterisation of Part-through Damage in a Stiffened Panel by a Time-reversal Based Imaging Method*, in *9th International Workshop on Structural Health Monitoring* 2013: Stanford University, Stanford, CA - USA.

[5] Chan, E., C.H. Wang, and L.R.F. Rose, *A Simplified Diffraction Tomography Method Incorporating Numerical Green's Functions for Imaging Structural Damage.* To be submitted, 2014.

[6] Hoon, S. and L. Sang Jun, *Lamb wave tuning curve calibration for surface-bonded piezoelectric transducers.* Smart Materials and Structures, 2010. **19**(1): p. 015007.

[7] Rose, L.R.F., C.H. Wang, and E. Chan, *A comparison and extension of algorithms for in-situ imaging of laminar damage in plates.* To be submitted, 2014.

[8] Wang, C.H. and L.R.F. Rose, *Minimum Sensor Density for Quantitative Damage Imaging*, in *9th International Workshop on Structural Health Monitoring* 2013: Stanford University, Stanford, CA - USA.

[9] Wang, C.H. and L.R.F. Rose, *Imaging Damage using Mixed Passive and Active Sensors*, in *4th Asia-Pacific Workshop on Structural Health Monitoring* 2012.

[10] Veidt, M., et al., *Imaging Laminar Damage in Plates Using Lamb Wave Beamforming.* Advanced Materials Research, 2008. **47**(50): p. 666-669.

[11] Hall, J.S. and J.E. Michaels. *Multi-path guided wave imaging for in situ montoring of complex structures*. in *Review of Progress in Quantitative Nondestructive Evaluation: Volume 32*. 2013. Denver, Colorado, USA.

[12] Anderson, B.E., et al., *Experimental implementation of reverse time migration for nondestructive evaluation applications.* The Journal of the Acoustical Society of America, 2011. **129**(1): p. EL8-EL14.